

AD-A193 126

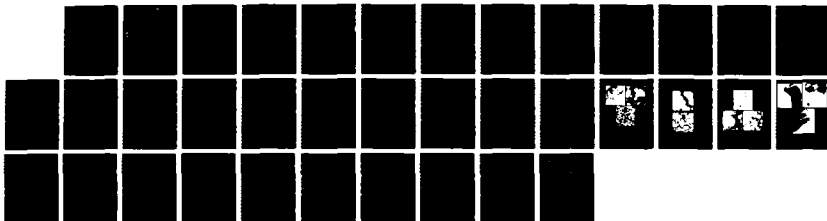
PROCESSING AND ADDITIVE EFFECTS OF ZR02 ON  
MICROSTRUCTURE AND DIELECTRIC. (U) ILLINOIS UNIV AT  
URBANA DEPT OF MATERIALS SCIENCE AND ENGINEE..  
T R ARMSTRONG ET AL. 28 DEC 87

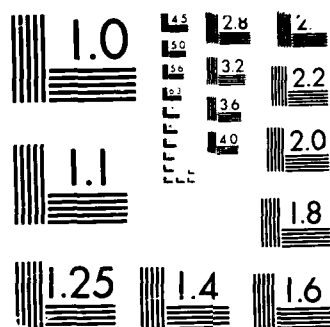
1/1

UNCLASSIFIED

F/G 20/3

NL





MICROCOPY RESOLUTION TEST CHART  
 (NBS 1963-A) STANDARDS 1963-A

DTIC FILE COPY

(Y)

AD-A193 126

Final Report  
Technical Report No. 14  
Contract No.: US NAVY-N-00014-80-K-0960  
N00014-87-K-0452

PROCESSING AND ADDITIVE EFFECTS OF  $ZrO_2$   
ON MICROSTRUCTURE AND DIELECTRIC PROPERTIES  
OF  $BaTiO_3$  CERAMICS

by

T. R. Armstrong, L. M. Morgens, A.K. Maurice  
and R. C. Buchanan

December 1987

Department of Materials Science and Engineering  
Ceramics Division  
University of Illinois at Urbana-Champaign  
105 So. Goodwin Ave.  
Urbana, IL 61801

Research was supported by the Office of Naval Research  
Metallurgy and Ceramics Program  
Department of the Navy

Production in whole or in part is permitted for  
any purpose of the United States Government

DECLASSIFICATION STATEMENT A

Approved for public release  
Distribution Unlimited

88 3 5 086

424193-126

## REPORT DOCUMENTATION PAGE

1a. REPORT SECURITY CLASSIFICATION Unclassified		1b. RESTRICTIVE MARKINGS	
2a. SECURITY CLASSIFICATION AUTHORITY		3. DISTRIBUTION/AVAILABILITY OF REPORT Widespread, required #'s of copies to defense documentation of individuals & organizations on approved distribution list furnished by Metallurgy & Cer. Prog. ONR	
2b. DECLASSIFICATION/DOWNGRADING SCHEDULE		4. PERFORMING ORGANIZATION REPORT NUMBER(S) Report #14	
5. MONITORING ORGANIZATION REPORT NUMBER(S)		6a. NAME OF PERFORMING ORGANIZATION University of Illinois	
6b. OFFICE SYMBOL (If applicable)		7a. NAME OF MONITORING ORGANIZATION	
6c. ADDRESS (City, State and ZIP Code) Department of Materials Science & Engineering Ceramics Division/204 Ceramics Bldg. 105 So. Goodwin, Urbana, IL 61801		7b. ADDRESS (City, State and ZIP Code)	
8a. NAME OF FUNDING/SPONSORING ORGANIZATION Office of Naval Research		8b. OFFICE SYMBOL (If applicable)	
9. PROCUREMENT INSTRUMENT IDENTIFICATION NUMBER		8c. ADDRESS (City, State and ZIP Code) Division of Materials Research Arlington, VA 22217	
10. SOURCE OF FUNDING NOS.		11. TITLE (Include Security Classification) Processing and Additive Effects of $ZrO_2$ on Microstructure & Dielectric Properties	
PROGRAM ELEMENT NO.		PROJECT NO.	
TASK NO.		WORK UNIT NO.	
12. PERSONAL AUTHOR(S) of $BaTiO_3$ Ceramics T. R. Armstrong and R. C. Buchanan		13a. TYPE OF REPORT Interim	
13b. TIME COVERED FROM 10/1/86 TO 10/1/87		14. DATE OF REPORT (Yr., Mo., Day) December 28, 1987	
15. PAGE COUNT 30		16. SUPPLEMENTARY NOTATION Powder processing effects in barium titanate.	
17. COSATI CODES		18. SUBJECT TERMS (Continue on reverse if necessary and identify by block number) Dielectrics, grain boundary modification, $BaTiO_3$ , zirconia processing.	
FIELD		GROUP	
SUB. GR.			
19. ABSTRACT (Continue on reverse if necessary and identify by block number)			

SEE NEXT PAGE

20. DISTRIBUTION/AVAILABILITY OF ABSTRACT UNCLASSIFIED/UNLIMITED <input checked="" type="checkbox"/> SAME AS RPT. <input type="checkbox"/> DTIC USERS <input type="checkbox"/>		21. ABSTRACT SECURITY CLASSIFICATION Unclassified	
22a. NAME OF RESPONSIBLE INDIVIDUAL		22b. TELEPHONE NUMBER (Include Area Code)	
		22c. OFFICE SYMBOL	

# ABSTRACT

SECURITY CLASSIFICATION OF THIS PAGE

Scanning Electron Microscopy

(Transmission Electron Microscopy)

> Dielectric properties and structure of  $\text{BaTiO}_3$  ceramics have been shown to be significantly influenced by small additions ( $< 2 \text{ wt\%}$ ) of  $\text{ZrO}_2$ . (SEM) and (TEM) observations revealed enhanced microstructural uniformity and retarded grain growth with  $\text{ZrO}_2$  addition, depending on sintering temperature ( $T_s$ ). For  $T_s < 1320^\circ\text{C}$ , TEM analysis showed  $\text{ZrO}_2$  at the grain boundaries as discrete particles ( $\sim 0.03 \mu\text{m}$ ) in a bandwidth of  $\pm 50 \text{ \AA}$ . Above  $1320^\circ\text{C}$ , diffusion of  $\text{ZrO}_2$  from the grain boundary region was observed, resulting in increased grain size and a tetragonal structure. X-ray diffraction analysis revealed a pseudo-cubic structure below  $1320^\circ\text{C}$  with both twinning and domain structure also suppressed. Ceramics with the pseudo-cubic structures showed a flattened dielectric constant response with temperature and significantly lower dielectric loss.



Accession For	
NPS 00001	<input checked="" type="checkbox"/>
DTIC 146	<input type="checkbox"/>
Unpublished	<input type="checkbox"/>
Distribution	
e. per ltr.	
Distribution	
Date	
Signature	
A-1	

SECURITY CLASSIFICATION OF THIS PAGE

## Table of Contents

	Page
I Introduction	1
II Experimental Procedure	3
III Results and Discussion	5
IV Conclusions	11
V Acknowledgements	11
VI References	12
VII List of Figures	15
VIII Technical Reports	29

# PROCESSING AND ADDITIVE EFFECTS OF $ZrO_2$ ON MICROSTRUCTURE AND DIELECTRIC PROPERTIES OF $BaTiO_3$ CERAMICS

T.R. Armstrong, L. M. Morgens, A. K. Maurice and R.C. Buchanan  
Department of Materials Science and Engineering  
University of Illinois at Urbana-Champaign, 61801

## I. INTRODUCTION

Ceramic capacitive components typically must have high permittivity for volumetric efficiency and a low temperature coefficient of capacitance for circuit performance. These capacitors are based primarily on ferroelectric compounds such as  $BaTiO_3$ , in which the desirable dielectric characteristics are obtained by incorporation of isovalent or aliovalent additives into the perovskite lattice as substitutions. In small concentrations, substitutions such as  $NiO$ ,  $ZrO_2$ ,  $Dy_2O_3$  and  $Nb_2O_5$ <sup>1,2</sup> may also act as grain growth inhibitors. These oxides modify the ferroelectric properties by controlling grain size and by suppressing or broadening the Curie peak. The Curie peak may be equally affected if substantial chemical inhomogeneity exists in the sintered material.<sup>3</sup>

Zirconia has been shown by Brajer<sup>4</sup> and Kulscar<sup>5</sup> to increase the orthorhombic-tetragonal transition temperature in  $BaTiO_3$  while slightly lowering the tetragonal-cubic transition. Hennings et al.<sup>6</sup> also noted this phenomenon and found that the permittivity increased to a broad maxima as the phase transition points con-

verged. Verbitskaia et al.<sup>7</sup> found that BaZrO<sub>3</sub> additions to BaTiO<sub>3</sub> had an effect on BaTiO<sub>3</sub> similar to ZrO<sub>2</sub> in that it decreased the axial ratio (c/a) of the tetragonal phase, in agreement with results by Kell and Hellicar.<sup>8</sup> Similar reductions, in the axial ratio have been achieved by additions of rare earth elements to BaTiO<sub>3</sub>.<sup>9,10</sup> In contrast, Molokhia and Issa<sup>11</sup> found that ZrO<sub>2</sub> additions increase the lattice parameters of BaTiO<sub>3</sub>,<sup>12</sup> with essentially no effect on the axial (c/a) ratio. Additionally, they observed that the dielectric constant exhibited a nonlinear behavior at low ZrO<sub>2</sub> concentration, while the dielectric losses decreased with increased ZrO<sub>2</sub> content. The nonlinearity of the dielectric constant has been attributed to the presence of Zr<sup>4+</sup> at interstitial positions at low zirconia concentrations, and on Ti<sup>4+</sup> sites at higher concentrations. Maurice<sup>13</sup> was able to prepare dense ceramic bodies from oxalate derived barium titanate which showed a flattened dielectric response to ZrO<sub>2</sub> additions  $\leq 2.0$  wt%. This behavior was attributed to ZrO<sub>2</sub> particulate accumulation at the grain boundaries. Armstrong and Buchanan<sup>14</sup> further determined that ZrO<sub>2</sub> resided primarily at the grain boundaries at sintering temperatures less than 1320°C.

Miller<sup>15</sup> and Kahn<sup>16</sup> have shown that grain growth in BaTiO<sub>3</sub> can also be inhibited by incorporation of additives such as carbon and niobium. Miller observed a variation in sintered density as a function of additive content. Kinoshinto and Yamaji<sup>17</sup> showed that as the grain size decreased the permittivity of the material increased and a general broadening of the transition peak resulted. Martirena and Burfoot<sup>18</sup> went a step further and suggested that the room temperature permittivity should markedly

increase when the transition region is suppressed. However Arlt et al.<sup>19</sup> showed that this was not always the case. In a recent study, Arlt showed that the room temperature permittivity decreased when the transition region became suppressed. Additionally, they determined from high angle x-ray analysis, as did Kahn<sup>16</sup>, that the degree of tetragonality decreased with grain size, giving rise to a pseudo-cubic structure at room temperature.

The objective of this investigation was to examine the effect of small additions of  $ZrO_2$  on the microstructure, dielectric properties and in particular the grain boundary structure of  $BaTiO_3$ . The work described here relates to unstabilized  $ZrO_2$  additions, primarily under sintering conditions where solid solubility was not fully achieved, assuring grain boundary residence of the additive.

## II. EXPERIMENTAL PROCEDURE

### (1) Sample Preparation

This study utilized commercial  $BaTiO_3^+$  of high purity with Ba/Ti atomic ratios of 0.997, 1.000 and 1.002, as determined by x-ray fluorescence analysis. The  $BaTiO_3$  powders were ball milled ( $ZrO_2$  media) with 0.0-2.0 wt% unstabilized  $ZrO_2^{++}$  additions. The average initial particle size of the  $BaTiO_3$  and  $ZrO_2$  powders was  $1.0\mu m$  and  $0.03\mu m$  respectively. Milling was carried out for 12h in a solution of 60 vol% isopropyl alcohol-deionized water

---

+ Ticon-HPB TAM Ceramics Inc., Niagara Falls, NY.

++ Zircar Products, Inc., Florida, NY.

with 1 wt% Menhadden fish oil<sup>+++</sup> added as a dispersant. Additions of PVA and Carbowax, 1 wt% each, were then made, followed by further milling (1.5h). The slurry was spray dried and the resulting powder uniaxially pressed into discs 16mm x 2mm at 136 MPa. Samples were sintered on ZrO<sub>2</sub> setter plates in air from 1275° to 1350°C for 1-3h. Densities of sintered compacts were measured both geometrically and by He pycnometry.

## (2) Characterization

After sintering, some compacts were crushed to an average particle size <40μm to achieve optimal random orientation for x-ray diffraction analysis. Diffraction analysis was carried out on the high angle (400)(004) and (200)(002) peaks, to determine the degree of tetragonality.<sup>19</sup> For dielectric measurements, the compacts were mechanically thinned with 600 grit SiC to achieve plane parallel surfaces, upon which Al electrodes were evaporated. Capacitance and loss measurements were made using an automatic capacitance bridge\* at 1 and 10 KHz. Bias field measurements (0-300 v/cm) were made with an external high voltage power supply\*\* in series with the capacitance bridge.

SEM microstructural examination were performed on as-fired and fracture surfaces sputtered with Pd-Au, using an ISI DS-130 electron microscope. Specimens for TEM/STEM (Philips EM 400 and 420/Vacuum Generators HB5) were prepared by mechanical

---

+++ Werner G. Smith Inc., Cleveland, Ohio

\* Model 4276A, Hewlett-Packard Co., Palo Alto, CA.

\*\* Model 241, Keithley Instrument Co., Cleveland, Ohio

polishing, using 15 $\mu$ m diamond grit and 6 $\mu$ m diamond paste, to a thickness of 120 $\mu$ m. The samples were further thinned and dimpled on both sides. Foils for TEM/STEM analysis were produced by ion beam thinning to perforation.

### III. RESULTS AND DISCUSSION

Addition of monoclinic ZrO<sub>2</sub> (0.5-2.0 wt%) to BaTiO<sub>3</sub> was found, in general, to decrease the density of the sintered compacts. Figure 1 shows the densities to increase with sintering temperature ( $T_s$ ) up to ~1320°C where maximum density was achieved for samples containing 0 and 2 wt% ZrO<sub>2</sub>. For samples with 1 wt% added ZrO<sub>2</sub> maximum density (~96%) was achieved at 1310°C. At higher sintering temperatures,  $T_s > 1320^\circ\text{C}$ , the densities for all samples decreased. This decrease has been attributed to increased inter-grannular porosity resulting from discontinuous grain growth at higher temperatures as described by Burke.<sup>20</sup>

The effects of ZrO<sub>2</sub> additions on the microstructure of BaTiO<sub>3</sub> are compared in the SEM photomicrographs of as-sintered surfaces (Figure 2) for samples sintered at 1320°C/2h. With no additive to BaTiO<sub>3</sub> (Figure 2a), a dense microstructure was observed consisting essentially of large grains (avg. GS ~50 $\mu$ m), with small grains distributed along the grain boundaries and intersections. With 1.0 wt% ZrO<sub>2</sub> addition (Figure 2b) the fraction of large grains decreased significantly, resulting in a bimodal distribution of large grains in a fine grain matrix. With 2.0 wt% ZrO<sub>2</sub> addition, a dense microstructure consisting entirely of uniform

small grains (avg. GS  $\sim 1.0\mu\text{m}$ ) was obtained. Figure 3 shows an identically similar trend for  $\text{BaTiO}_3$  samples sintered at  $1300^\circ\text{C}/2\text{h}$ , except that here only 1.0 wt%  $\text{ZrO}_2$  was needed to suppress the grain growth.

Figure 4 shows the progression of microstructural development (1.0 wt%  $\text{ZrO}_2$  added to  $\text{BaTiO}_3$ ) as a function of sintering temperature from  $1310$ – $1350^\circ\text{C}$  for a 2h soak time. The SEM photomicrographs show uniform grain size structures for the  $1310^\circ\text{C}$  and  $1350^\circ\text{C}$  samples with significantly larger grain size for the latter. In contrast, the intermediate temperature at  $1320^\circ\text{C}$  showed a transition bimodal structure again consisting of large grains in a fine grain matrix. It is clear that the addition of  $\text{ZrO}_2$  to  $\text{BaTiO}_3$  suppresses grain growth. However, increasing amounts of  $\text{ZrO}_2$  (0.5–2.0 wt%) were needed for the suppression of grain growth as the sintering temperature increased from 1300 to  $1350^\circ\text{C}$ , indicating progressive solubility of  $\text{ZrO}_2$  in the  $\text{BaTiO}_3$  lattice.

TEM analysis of  $\text{BaTiO}_3$  with added  $\text{ZrO}_2$  revealed the presence of  $\text{ZrO}_2$  along the grain and pore boundaries for  $T_s \leq 1310^\circ\text{C}/2\text{h}$ , (1.0 wt%  $\text{ZrO}_2$ ) as shown in Figure 5a. The  $\text{ZrO}_2$  appeared as discrete particles ( $\sim 0.03\mu\text{m}$ ), which corresponded to the initial particle size of the added  $\text{ZrO}_2$ . However, distribution along the boundaries was not uniform. EDS analysis of these boundary regions revealed a Zr bandwidth of  $\pm 50\text{\AA}$  in samples containing 1 wt%  $\text{ZrO}_2$  and sintered at  $1300^\circ\text{C}$ . As shown in Figure 6, the Zr bandwidth increased to  $\sim \pm 100\text{\AA}$  at  $1310^\circ\text{C}$ . In contrast, TEM evaluation of samples sintered at  $1320^\circ\text{C}$  and  $1350^\circ\text{C}$  (1.0 wt%  $\text{ZrO}_2$ ) showed only small discrete regions of  $\text{ZrO}_2$  at the grain boundaries and at triple points (Figures 5b, 5c). For the

1350°C sample, the approximate particle size of the residual  $\text{ZrO}_2$  was found to be about 90Å, and a broader, less defined Zr bandwidth was observed. The diminished concentration of inter-grannular  $\text{ZrO}_2$  particles along with its smaller size and wider bandwidth indicated diffusion of Zr into the  $\text{BaTiO}_3$  lattice at  $T_s \geq 1320^\circ\text{C}$ , leaving insufficient residual  $\text{ZrO}_2$  to inhibit grain boundary motion. Interestingly, this is also the approximate temperature for the formation of a liquid phase in the  $\text{BaTiO}_3$  system, evident also along grain boundaries in Figure 5. This condition would aid solubility and material transport.

The large grains evident in Figures 2 to 5, typically showed a well developed domain structure with frequent twinning. Detailed analysis of the microstructure by TEM/STEM revealed a reduction in the formation of  $\langle 111 \rangle$  twins as the grain size decreased, due either to the presence of  $\text{ZrO}_2$  or to a decrease in the sintering temperature. However, the presence of zirconia at the grain boundaries did not significantly disrupt or alter the existing domain structure of the grains (Figure 5a,5b). This may be due to the small amount of  $\text{ZrO}_2$  present at the grain boundaries and to limited  $\text{Zr}^{4+}$  diffusion into the lattice. However, as the grain size decreased the domain structure also decreased with the grains tending to be single domains.

High angle x-ray diffraction analysis of the samples showed progve development of a pseudo-cubic structure as a function of added  $\text{ZrO}_2$ , reduced sintering temperature and smaller grain size. At grain sizes  $>5\mu\text{m}$  in undoped  $\text{BaTiO}_3$  the axial ratio ( $c/a$ ) was measured to be 1.011. Upon addition of  $\text{ZrO}_2$  the axial ratio decreased to 1.005 for samples of comparative grain size. As the

grain size decreased to  $0.7\mu\text{m}$  at  $T_s=1300^\circ\text{C}$ , the pseudo-cubic structure, characterized by two broad reflections centered at  $100.9^\circ 2\theta$ , with no distinct splitting in the (400)(004) peaks, became fully developed (Figure 7). Table 1 shows this data and the lattice parameter changes for different  $\text{ZrO}_2$  concentrations and sintering temperatures. The pseudo-cubic structure modification was also found to be particularly well developed for the optimally dense and small grain size samples with 1.0 wt%  $\text{ZrO}_2$  ( $1310^\circ\text{C}/2\text{h}$ ) and 2.0 wt%  $\text{ZrO}_2$  ( $1320^\circ\text{C}/2\text{h}$ ).

The observed trends in grain size and x-ray data are in agreement with previous studies.<sup>7,8</sup> For  $T_s=1350^\circ\text{C}$  it is apparent that the added  $\text{ZrO}_2$  causes a decrease in the axial ratio of  $\text{BaTiO}_3$ , which can be attributed to the incorporation of  $\text{ZrO}_2$  into the  $\text{BaTiO}_3$  lattice. However, for  $T_s<1350^\circ\text{C}$ ,  $\text{ZrO}_2$  acts increasingly as a grain growth inhibitor, decreasing grain size and distorting the perovskite lattice depending on concentration. The formation of the pseudo-cubic perovskite structure, therefore, is an effect of the decreasing grain size as described by Arlt.<sup>19</sup>

Dielectric data as a function of temperature for the  $\text{BaTiO}_3$  samples (0-2.0 wt% added  $\text{ZrO}_2$ ,  $T_s=1320^\circ\text{C}/2\text{h}$ ) are presented in Figure 8. Room temperature permittivity values are seen to increase with added  $\text{ZrO}_2$  (relative to the undoped  $\text{BaTiO}_3$ ) except for samples with 1.0 wt%  $\text{ZrO}_2$  which showed a decrease in permittivity. This is probably due to the highly bimodal microstructure of the 1.0 wt%  $\text{ZrO}_2$  sample, compared to the more uniform grain size microstructures depicted in Figure 2. As expected, the smaller grain size microstructures (2.0 wt% added  $\text{ZrO}_2$ ) showed the highest permittivity values,<sup>17</sup> with a near complete suppression of

the Curie peak for the tetragonal-cubic transition at  $\sim 125^{\circ}\text{C}$ . In contrast, samples with lower  $\text{ZrO}_2$  concentration showed a fully developed tetragonal structure as indicated by the sharp Curie peaks.  $\tan\delta$  values showed an essentially linear decrease with temperature for both 2.0 and 0.5 wt% added  $\text{ZrO}_2$  except for the existence of small transition peaks in the latter sample. For the 1.0 and 0.0 wt%  $\text{ZrO}_2$  samples the transition peaks were more pronounced but  $\tan\delta$  was less than 4% at room temperature. Both  $\tan\delta$  and dielectric constant showed clearly the expected increase in the orthorhombic-tetragonal and corresponding decrease in the tetragonal-cubic transition temperatures.<sup>5,6</sup> This is another indication that  $\text{ZrO}_2$  is going into solid solution in the  $\text{BaTiO}_3$  at  $1320^{\circ}\text{C}$ . Figure 9 shows the dielectric behavior of ceramics with optimally dense fine grained microstructures obtained at  $1310^{\circ}\text{C}$  and  $1320^{\circ}\text{C}$ , with a 2h soak. The samples show full Curie peak suppression and linear  $\tan\delta$ , decreasing with temperature. The somewhat higher permittivities and  $\tan\delta$  values for the  $1320^{\circ}\text{C}$  sample reflect the higher density and  $\text{ZrO}_2$  solubility.

In line with the microstructures shown in Figures 3 and 4, the samples fired at  $1300^{\circ}\text{C}$  showed high permittivities and an essentially flat dielectric response with temperature between room temperature and  $120^{\circ}\text{C}$  as depicted in Figure 10. However, with increased sintering temperature the permittivity values decreased, for the same added  $\text{ZrO}_2$  content (1.0 wt%) reflecting progressively larger grain size development and increasing  $\text{ZrO}_2$  solubility in the perovskite lattice. The relatively low permittivity for ceramics with  $T_s=1350^{\circ}\text{C}$  reflected further the relatively low density

of the sample. Dissipation factor trends were again similar to the trends in Figure 8.

Summarizing the dielectric data for  $\text{BaTiO}_3$  with small  $\text{ZrO}_2$  additions, it can be concluded that the dominant effect was grain size. With smaller grain size higher permittivities were observed as well as lower dielectric losses. This grain size suppression corresponded to the condition of  $\text{ZrO}_2$  being resident at the grain boundaries. In cases where  $\text{ZrO}_2$  diffused into the lattice, a shift in the Curie transition peak was observed and also a slight increase in permittivity. These observations are reflected in the data given in Figure 11 which shows the change in capacitance with bias field for the different samples. Ceramics with more uniform, fine grain microstructures generally showed smaller capacitance deviation with applied bias field, indicative also of lower dissipation factors and higher insulation resistance.

Figure 12 shows the stoichiometry effect on the dielectric properties of the doped  $\text{BaTiO}_3$  samples. The samples compared were sintered at  $1300^\circ\text{C}/2\text{h}$  and had 1.0 wt% added  $\text{ZrO}_2$ . These specimens all showed a flattened dielectric response above the orthorhombic-tetragonal transition and a low  $\tan\delta$  which decreased linearly with temperature. The samples with atomic ratios  $<1.000$  showed higher permittivity values, this effect being due to the samples having higher density and smaller grain size.<sup>21</sup> No difference was observed in the dielectric response of samples with atomic ratios  $>1.000$ , within the stoichiometric range examined. The  $\tan\delta$  for all three samples was observed to decrease linearly with temperature and showed little significant variation.

#### IV. CONCLUSIONS

1. Unstabilized (monoclinic)  $\text{ZrO}_2$  added to  $\text{BaTiO}_3$  (0.5-2.0 wt%, sintered at 1300-1350°C/1-2h) was found to result in:  
a) suppression of grain growth with  $\text{ZrO}_2$  resident at the grain boundaries and, b) diffusion into the perovskite lattice at higher sintering temperatures, resulting in increased permittivity and convergence of the orthorhombic-tetragonal and tetragonal-cubic transition temperatures.
2. For case (a) the tetragonal-cubic transition peak was suppressed, resulting in an essentially flat dielectric constant profile to room temperature and a linear decrease from 25° to -55°C. Dissipation factor values were much reduced for these samples.
3. Suppression of the Curie peak as described above, coincided with a suppression of the cubic-tetragonal transition resulting in a pseudo-cubic structure characterized by a reduced c/a ratio.
4. Stoichiometry effects of the  $\text{ZrO}_2$  addition to  $\text{BaTiO}_3$  were relatively insignificant for conditions where the added  $\text{ZrO}_2$  was resident at the grain boundaries.

#### V. Acknowledgments

This work was supported by the Office of Naval Research under contract No. N-00014-80-K-0969 and in part by the National Science Foundation under MRL Grant DMR-86-12860.

## VI. References

1. G. Goodman, "Ceramic Capacitor Materials," Ceramic Materials for Electronics, Ch. 2, Ed. by R. C. Buchanan, Marcel Dekker Inc. New York (1986).
2. Y. Enomoto and A. Yamaji, "Preparation of Uniformly Small-Grained  $\text{BaTiO}_3$ ," Am. Ceram. Soc. Bull., 60 [5] 566-70 (1981).
3. D. Hennings and G. Rosenstein, "Temperature-Stable Dielectrics Based on Chemically Inhomogeneous  $\text{BaTiO}_3$ ," J. Am. Ceram. Soc., 67 [4] 249-54 (1984).
4. E. J. Brajer, "Polycrystalline Ceramic Material," U.S. Pat. No. 2,708,243 (1955).
5. F. Kulscar, "Fired Ceramics Barium Titanate Body," U.S. Pat. No. 2,735,024 (1956).
6. D. Hennings, A. Schnell and G. Simon, "Diffuse Ferroelectric Phase Transitions in  $\text{Ba}(\text{Ti}_{1-y}\text{Zr}_y)\text{O}_3$  Ceramics," J. Am. Ceram. Soc., 65 [11] 539-44 (1982).
7. T. N. Verbitskaia, G. S. Zhdanov, Iu. N. Venevtsev and S. P. Soloviev, "Electrical and X-ray Diffraction Studies of the  $\text{BaTiO}_3$ - $\text{BaZrO}_3$  System," Sov. Phy-Cryst., 3 [2] 182-92 (1958).
8. R. C. Kell and N. J. Hellicar, "Structural Transitions in Barium Titanate-Zirconate Transducer Materials," Acustica, 6 [2] 235-38 (1956).
9. N. M. Molakhia, M. A. Issa and S. A. Nasser, "Dielectric and X-ray Diffraction Studies of Barium Titanate Doped with Ytterbium," J. Am. Ceram. Soc., 67 [4] 289-91 (1984).

10. A. Yamaji, Y. Enomoto, K. Kinoshita and T. Murakami, "Preparation, Characterization and Properties of Dy-Doped Small-Grained BaTiO<sub>3</sub>," J. Am. Ceram. Soc., 64 [3-4] 97-101 (1977).
11. N. M. Molokhia and M. A. Issa, "Dielectric Properties of BaTiO<sub>3</sub> Modified with ZrO<sub>2</sub>," Pramana, 11 [3] 289-93 (1978).
12. G. H. Jonker and W. Kwestroo, "The Ternary Systems BaO-TiO<sub>2</sub>-SnO<sub>2</sub> and BaO-TiO<sub>2</sub>-ZrO<sub>2</sub>," J. Am. Ceram. Soc., 41 [10] 390-94 (1958).
13. A. K. Maurice, "Powder Synthesis, Stoichiometry, and Processing Effects on Properties of High Purity Barium Titanate," M.S. Thesis, University of Illinois (1984).
14. T. R. Armstrong and R. C. Buchanan, "Influence of ZrO<sub>2</sub> on the Microstructure of BaTiO<sub>3</sub>," Proceedings of the 45<sup>th</sup> Annual Meeting of EMSA, Baltimore, MD, pp.378-9 (1987).
15. A. Miller, "High Density Sintering of Pure Barium Titanate," J. Mat. Sci., 3 436-9 (1968).
16. M. Kahn, "Effects of Sintering and Grain Growth Reactions on the Distribution of Niobium Additive in Barium Titanate Ceramics," PhD. Thesis, Penn State University (1969).
17. K. Kinoshita and A. Yamaji, "Grain-Size Effects on Dielectric Properties in Barium Titanate," J. Appl. Phys., 47 [1] 371-4 (1976).
18. H. T. Martirena and J. C. Burfoot, "Grain-Size Effects on Properties of Some Ferroelectrics Ceramics," J. Phys. Soc. C., 7 3182-92 (1974).
19. G. Arlt, D. Hennings, and G. de With, "Dielectric Properties of Fine-Grained Barium Titanate Ceramics," J. Appl. Phys., 58 [4] 1619-25 (1985).

20. J. E. Burke, "Recrystallization and Sintering in Ceramics," Ceramic Fabrication Processes, Ed. by W. D. Kingery, John Wiley and Sons, New York 120-30 (1958).
21. A. K. Maurice and R. C. Buchanan, "Preparation and Stoichiometry Effects on Microstructure and Properties of High Purity  $\text{BaTiO}_3$ ," Ferroelectrics, 74 61-75 (1987).

## VII. List of Figures

- Figure 1. Fired density (%ThD) as a function of sintering temperature for  $\text{BaTiO}_3$  modified with 0-2.0 wt% monoclinic  $\text{ZrO}_2$ .
- Figure 2. The effect of added monoclinic zirconia on grain size for  $\text{BaTiO}_3$  ( $\text{Ba/Ti}=0.997$ ) samples sintered at  $1320^\circ\text{C}/2\text{h}$ : a) 0.0 wt% added  $\text{ZrO}_2$ , b) 1.0 wt% and c) 2.0 wt%.
- Figure 3. Effect of added zirconia (1.0 wt%) on grain size inhibition of  $\text{BaTiO}_3$  ( $\text{Ba/Ti}=1.002$ ) sintered at  $1300^\circ\text{C}/2\text{h}$ : a) 0.0 wt% added  $\text{ZrO}_2$  and b) 1.0 wt%  $\text{ZrO}_2$ .
- Figure 4. The effect of sintering temperature on densification and microstructure of  $\text{BaTiO}_3$  ( $\text{Ba/Ti}=0.997$ ) samples with 1.0 wt%  $\text{ZrO}_2$ : a)  $1310^\circ\text{C}/2\text{h}$ , b)  $1320^\circ\text{C}/2\text{h}$  and  $1350^\circ\text{C}/2\text{h}$ .
- Figure 5. TEM photomicrographs showing progressive dissolution of  $\text{ZrO}_2$  (1.0 wt%) along  $\text{BaTiO}_3$  ( $\text{Ba/Ti}=0.997$ ) grain boundaries with increasing sintering temperature: a)  $1310^\circ\text{C}/2\text{h}$ , b)  $1320^\circ\text{C}/2\text{h}$  and c)  $1350^\circ\text{C}/2\text{h}$ .
- Figure 6. EDS profile of grain boundary region in  $\text{BaTiO}_3$  (1.0 wt% added  $\text{ZrO}_2$ ) sintered at  $1310^\circ\text{C}/2\text{h}$ , showing Zr distribution around grain boundary.
- Figure 7. High angle x-ray diffraction pattern of  $\text{BaTiO}_3$  with 1.0 wt%  $\text{ZrO}_2$  showing progressive suppression of the tetragonal (400) and (004) peaks as sintering temperature is decreased.
- Figure 8. Dielectric response of 0.0, 0.5, 1.0 and 2.0 wt% zirconia additions to  $\text{BaTiO}_3$  sintered at  $1320^\circ\text{C}/2\text{h}$  (10kHz).

Figure 9. Dielectric response of  $\text{BaTiO}_3$  with optimal zirconia concentrations of 0.5 wt% 1310 $^\circ$ /2h and 2.0 wt% 1320 $^\circ$ /2h at 10kHz.

Figure 10. Dielectric spectra for  $\text{BaTiO}_3$  (1.0 wt% added  $\text{ZrO}_2$ ) samples sintered at 1300, 1310, 1320 and 1350 $^\circ\text{C}$  for 2h.

Figure 11. Change in capacitance as a function of bias field for  $\text{BaTiO}_3$  with 1.0 wt% added zirconia.

Figure 12. Dielectric response of  $\text{BaTiO}_3$  (1.0 wt% added  $\text{ZrO}_2$ ) with varying Ba/Ti atomic ratios 0.997, 1.000 and 1.002 sintered at 1300 $^\circ\text{C}$ /2h.

TABLE I. EFFECT OF ADDED ZIROCNIA ON THE AXIAL RATIO OF BaTiO<sub>3</sub>

SAMPLE	PEAK	a(Å)	c(Å)	c/a
BaTiO <sub>3</sub> (Ba/Ti=0.997)	(200,002)	3.009	4.038	1.011
PLUS ZrO <sub>2</sub> (1300°C/1h)				
0.5 wt%	(400,004)	NO SPLITTING*		
1.0 wt%	(400,004)	NO SPLITTING		
2.0 wt%	(400,004)	NO SPLITTING		
(1310°C/2h)				
0.5 wt%	(400,004)	NO SPLITTING		
1.0 wt%	(400,004)	NO SPLITTING		
(1320°C/2h)				
1.0 wt%	(400,004)	3.993	4.009	1.004
2.0 wt%	(400,004)	NO SPLITTING		
(1350°C/1h)				
1.0 wt%	(400,004)	3.992	4.010	1.005
2.0 wt%	(400,004)	4.005	4.025	1.005

\* Indicates pseudo-cubic modification

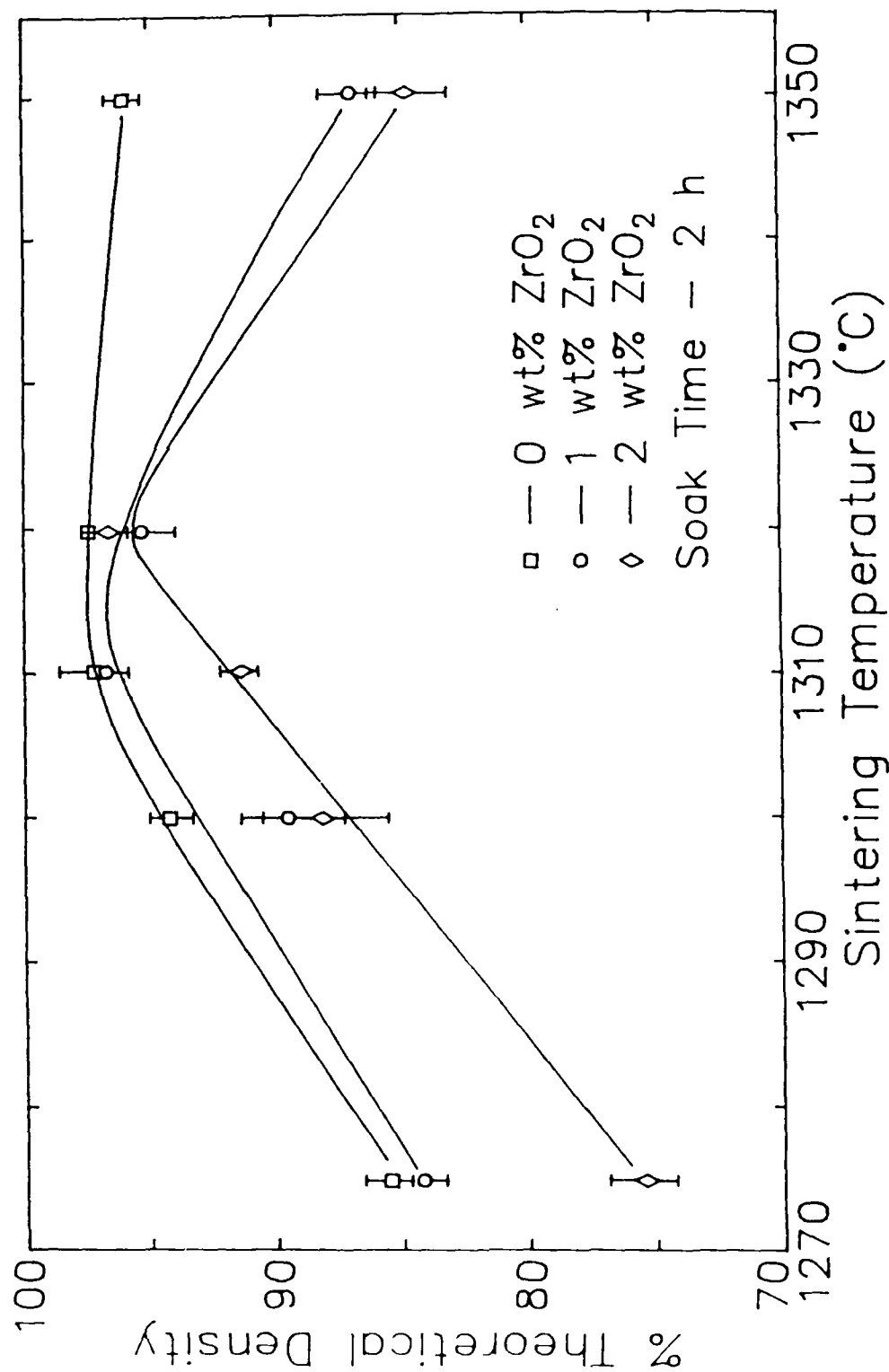


Figure 1. Fired density (%ThD) as a function of sintering temperature for  $\text{BaTiO}_3$  modified with 0-2.0 wt% monoclinic  $\text{ZrO}_2$ .

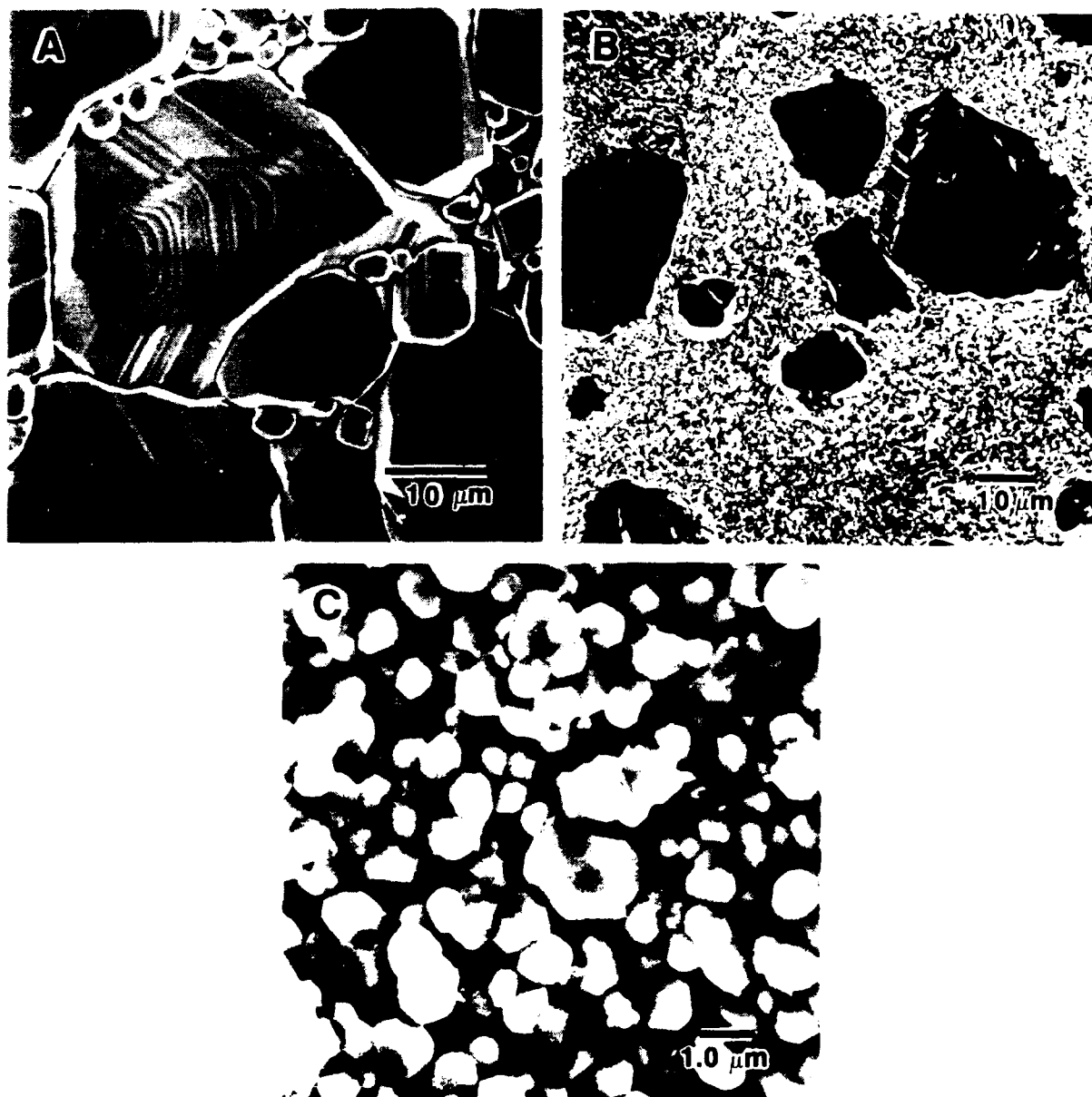


Figure 2. The effect of added monoclinic zirconia on grain size for  $\text{BaTiO}_3$  ( $\text{Ba}/\text{Ti}=0.997$ ) samples sintered at  $1320^\circ\text{C}/2\text{h}$ : a) 0.0 wt% added  $\text{ZrO}_2$ , b) 1.0 wt% and c) 2.0 wt%.

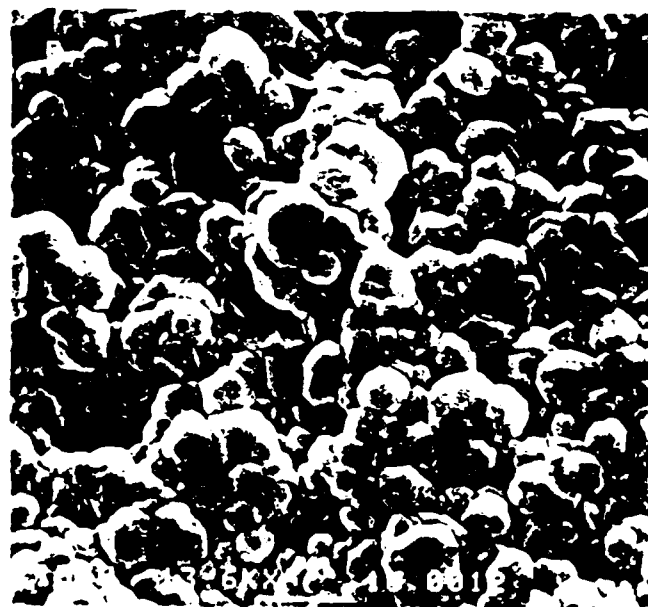
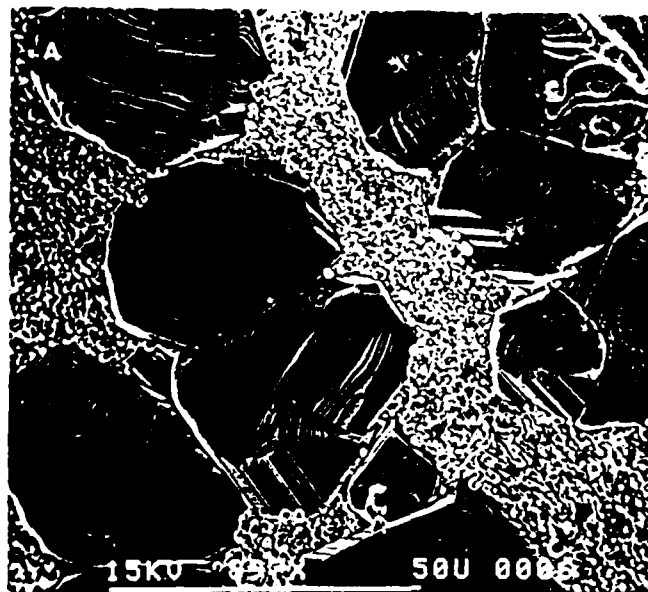


Figure 3. Effect of added zirconia (1.0 wt%) on grain size inhibition of  $\text{BaTiO}_3$  ( $\text{Ba/Ti}=1.002$ ) sintered at  $1300^\circ\text{C}/2\text{h}$ : a) 0.0 wt% added  $\text{ZrO}_2$  and b) 1.0 wt%  $\text{ZrO}_2$ .

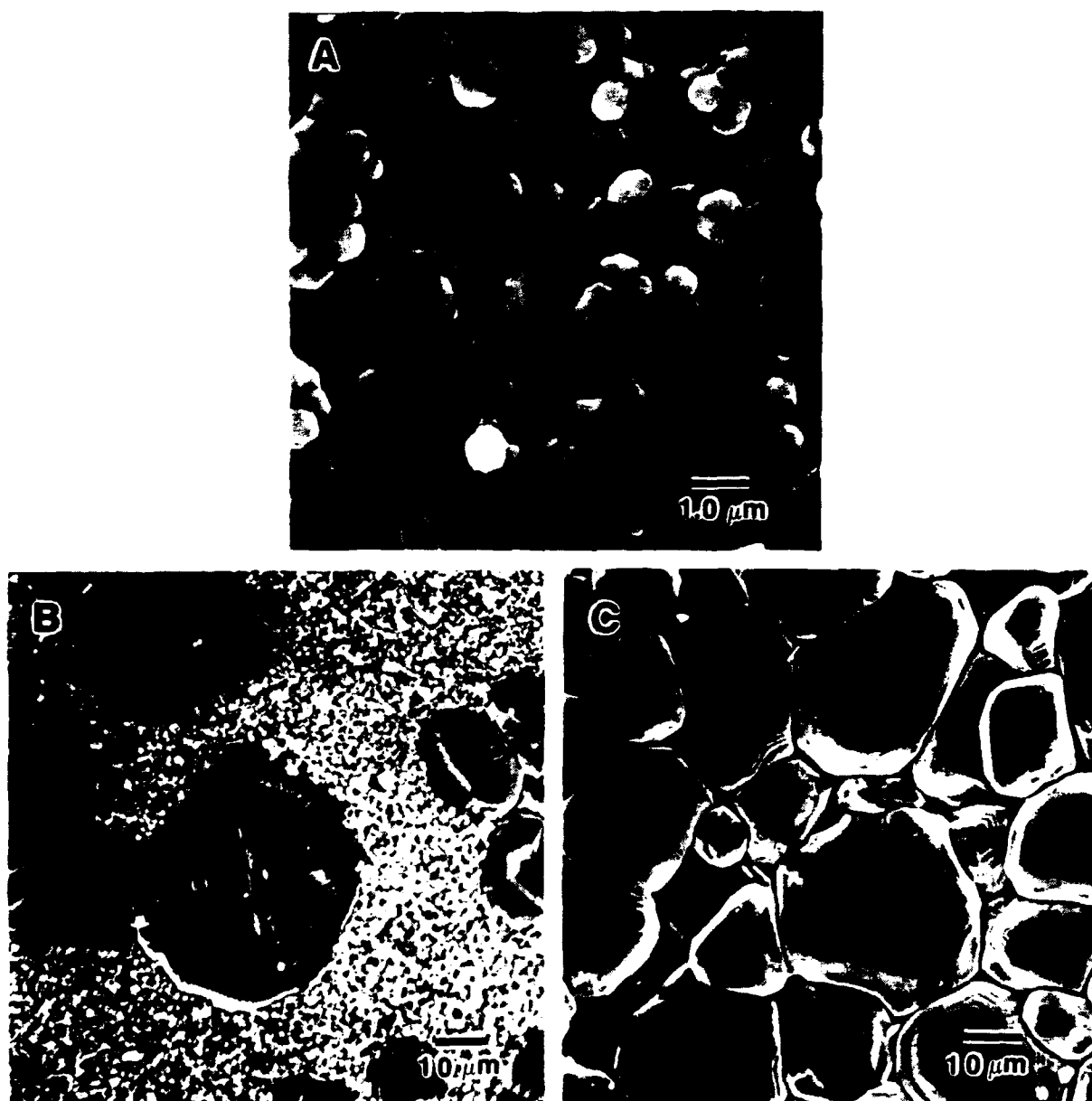


Figure 4. The effect of sintering temperature on densification and microstructure of  $\text{BaTiO}_3$  ( $\text{Ba/Ti}=0.997$ ) samples with 1.0 wt%  $\text{ZrO}_2$ : a)  $1310^\circ\text{C}/2\text{h}$ , b)  $1320^\circ\text{C}/2\text{h}$  and  $1350^\circ\text{C}/2\text{h}$ .

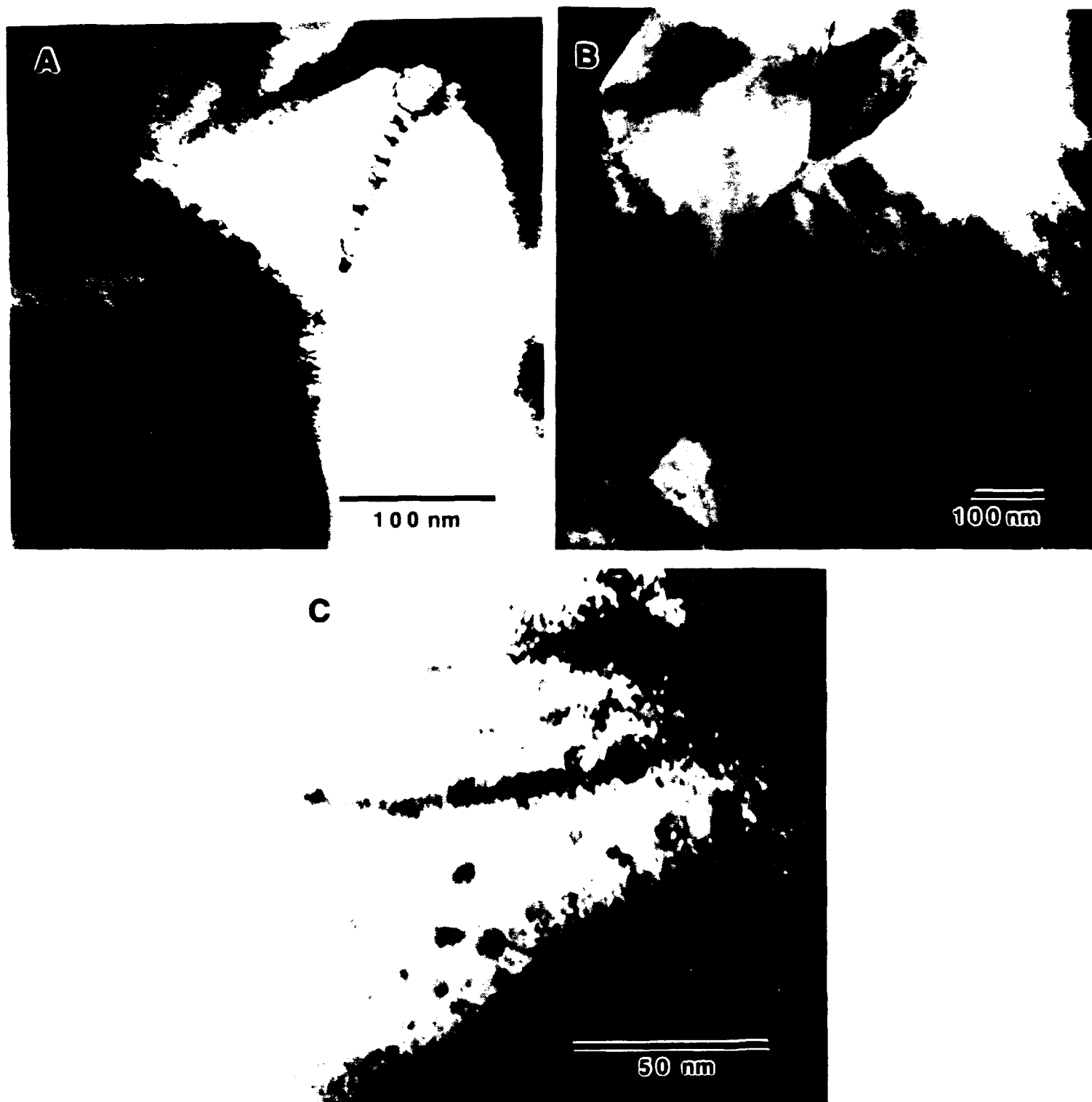
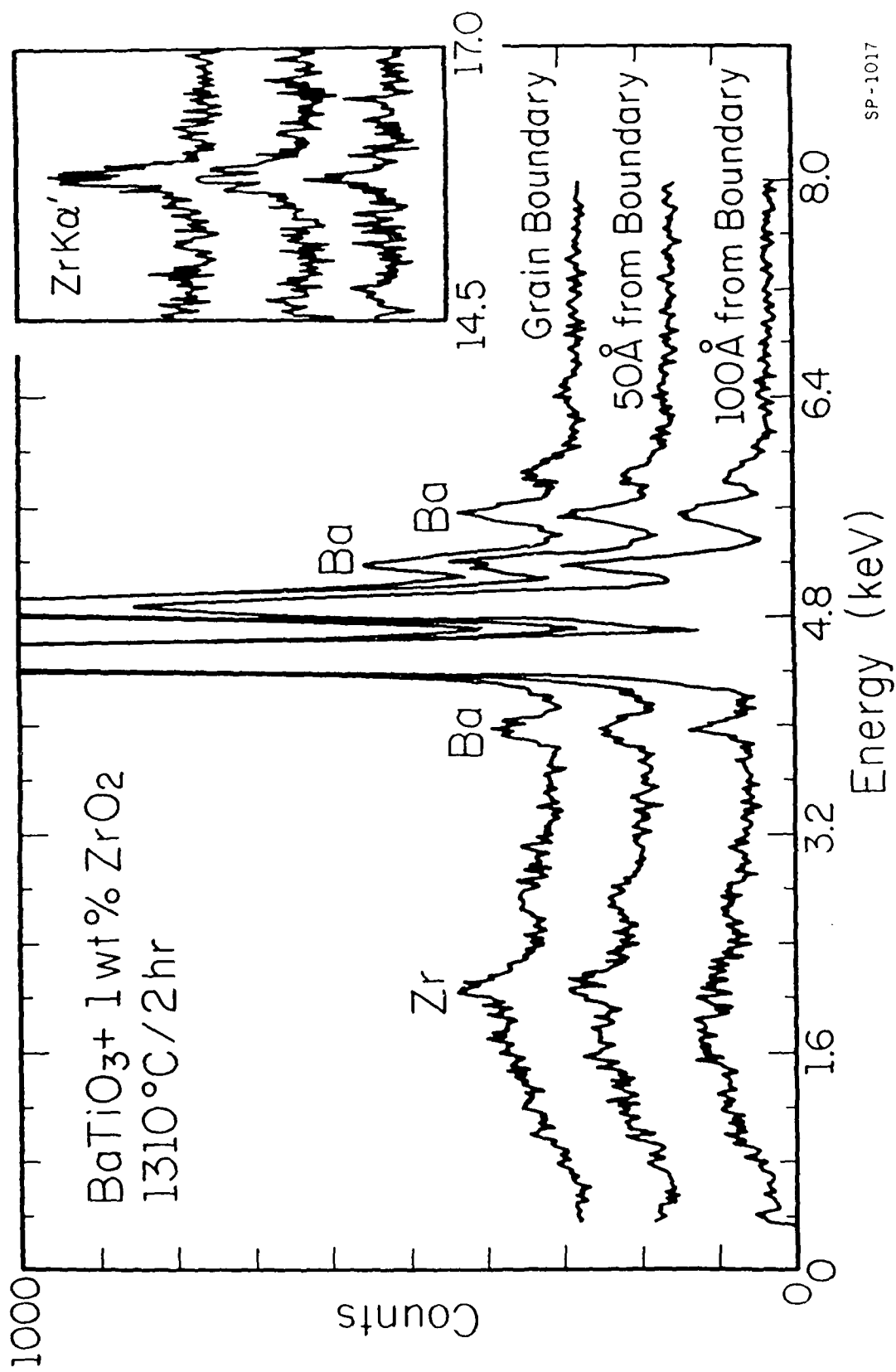


Figure 5. TEM photomicrographs showing progressive dissolution of  $\text{ZrO}_2$  (1.0 wt%) along  $\text{BaTiO}_3$  ( $\text{Ba/Ti}=0.997$ ) grain boundaries with increasing sintering temperature: a)  $1310^\circ\text{C}/2\text{h}$ , b)  $1320^\circ\text{C}/2\text{h}$  and c)  $1350^\circ\text{C}/2\text{h}$ .



SP-1017

Figure 6. EDS profile of grain boundary region in  $\text{BaTiO}_3$  (1.0 wt% added  $\text{ZrO}_2$ ) sintered at  $1310^\circ\text{C}/2\text{h}$ , showing Zr distribution around grain boundary.

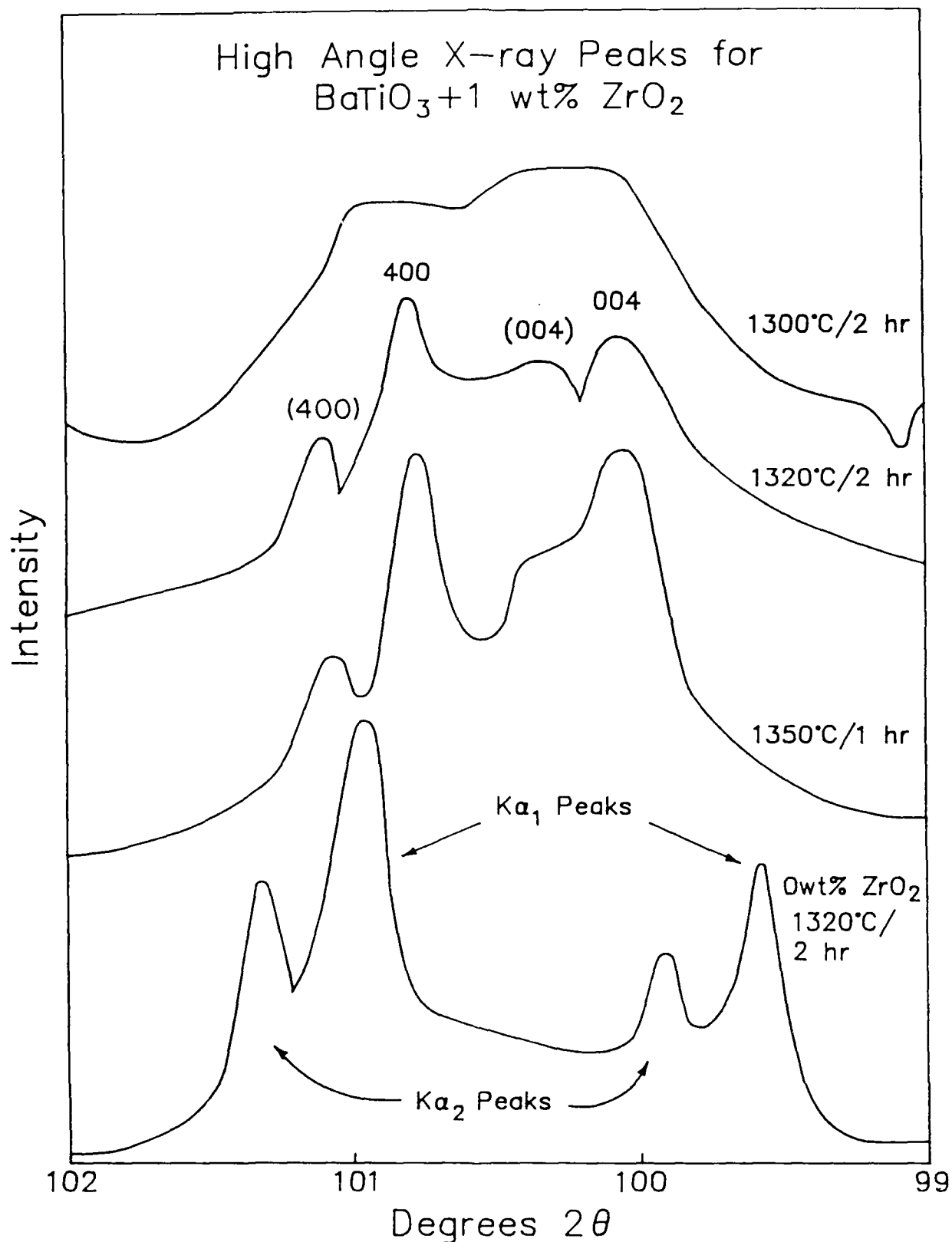


Figure 7. High angle x-ray diffraction pattern of  $\text{BaTiO}_3$  with 1.0 wt%  $\text{ZrO}_2$  showing progressive suppression of the tetragonal (400) and (004) peaks as sintering temperature is decreased.

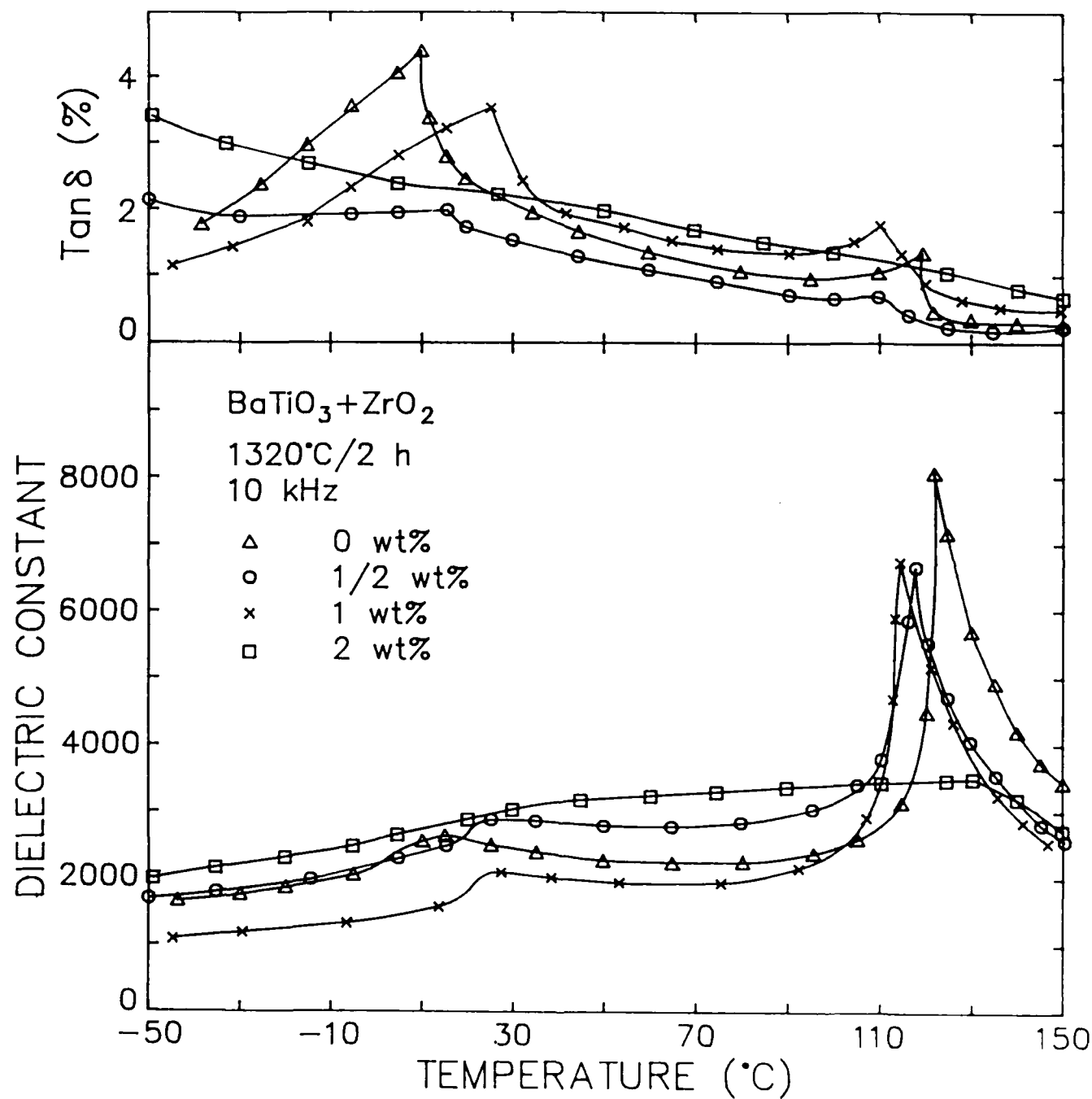


Figure 8. Dielectric response of 0.0, 0.5, 1.0 and 2.0 wt% zirconia additions to  $\text{BaTiO}_3$  sintered at 1320°C/2h (10kHz).

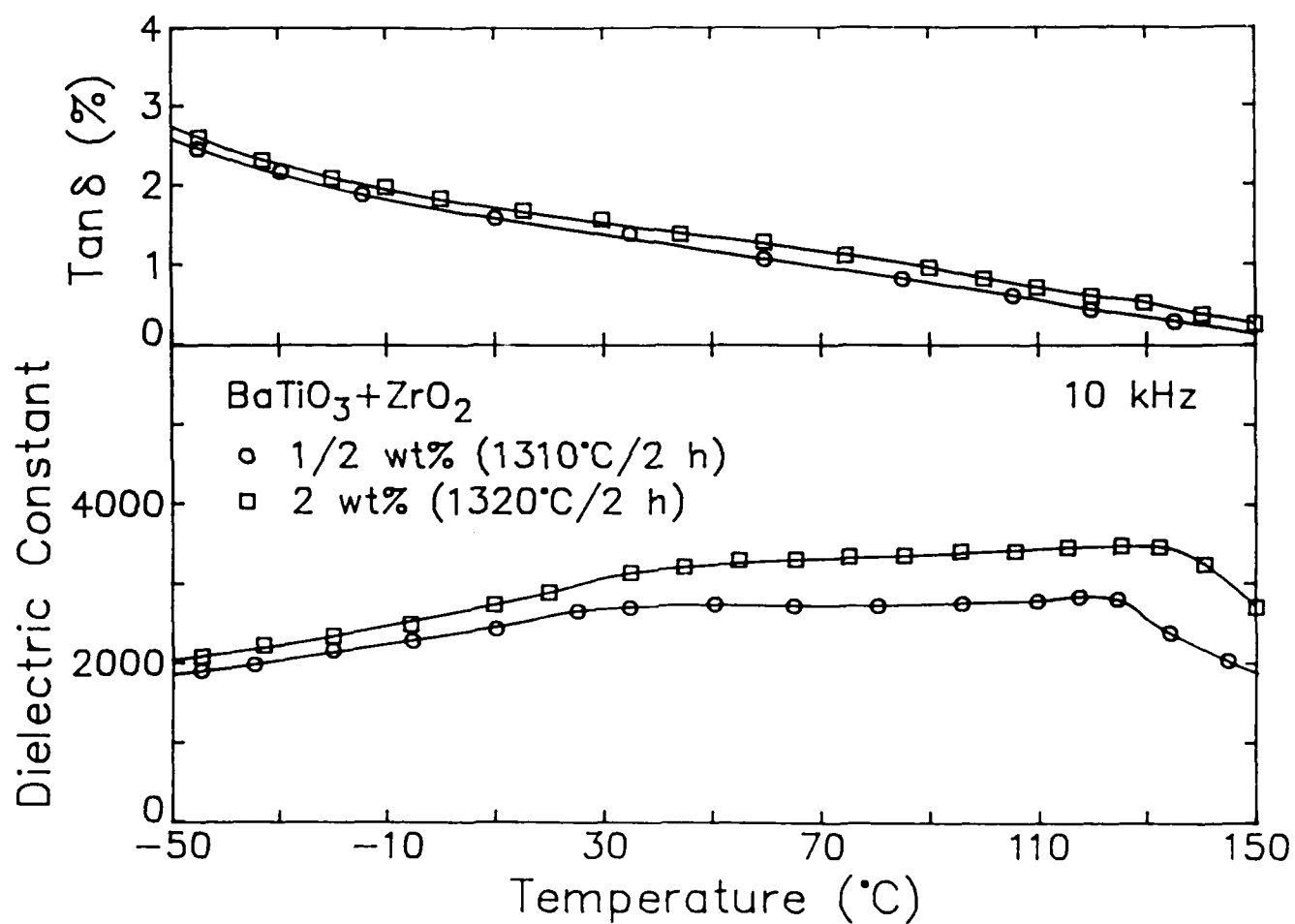


Figure 9. Dielectric response of  $\text{BaTiO}_3$  with optimal zirconia concentrations of 0.5 wt% 1310°C/2h and 2.0 wt% 1320°C/2h at 10kHz.

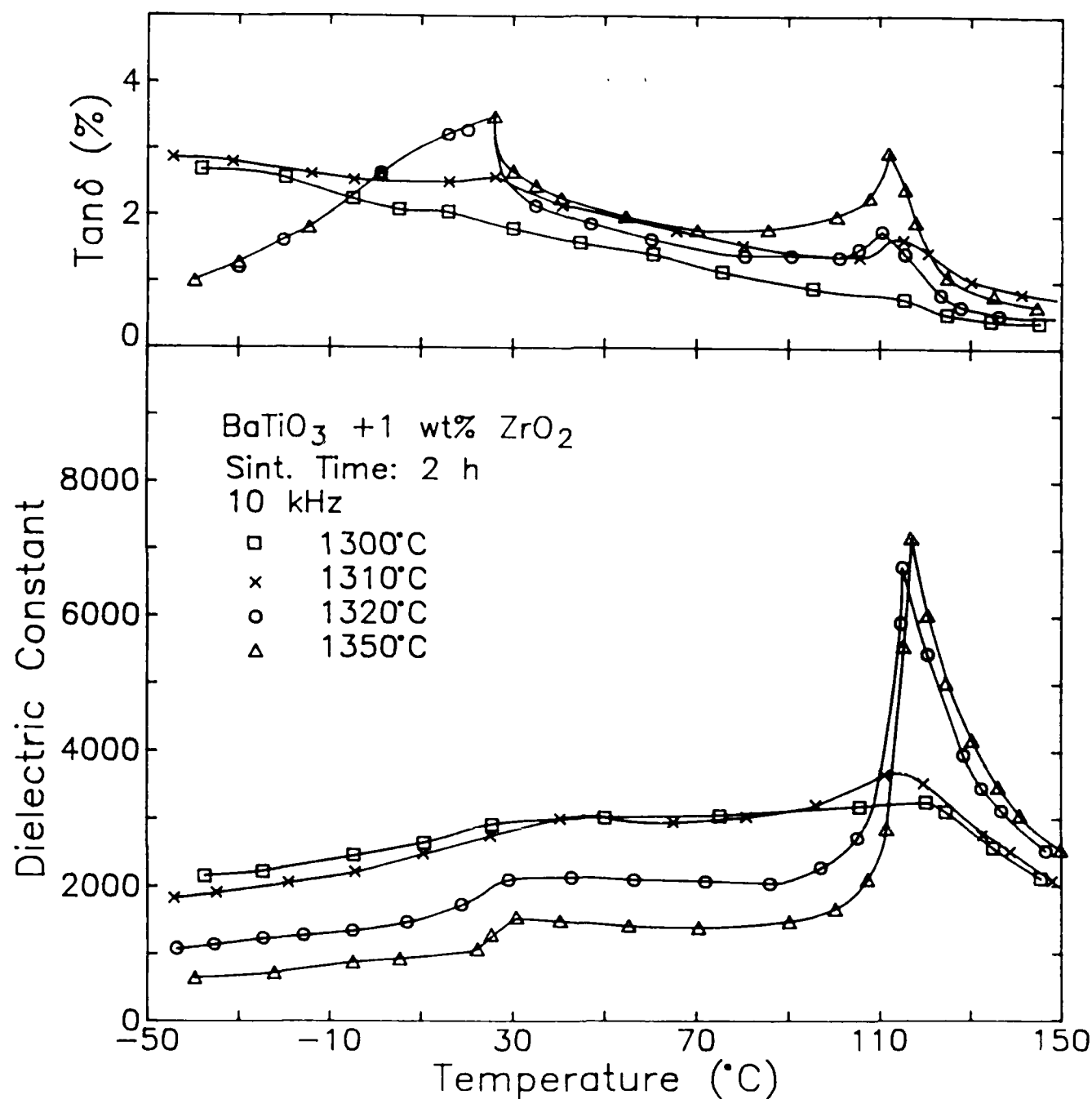


Figure 10. Dielectric spectra for  $\text{BaTiO}_3$  (1.0 wt% added  $\text{ZrO}_2$ ) samples sintered at 1300, 1310, 1320 and 1350 $^{\circ}\text{C}$  for 2h.

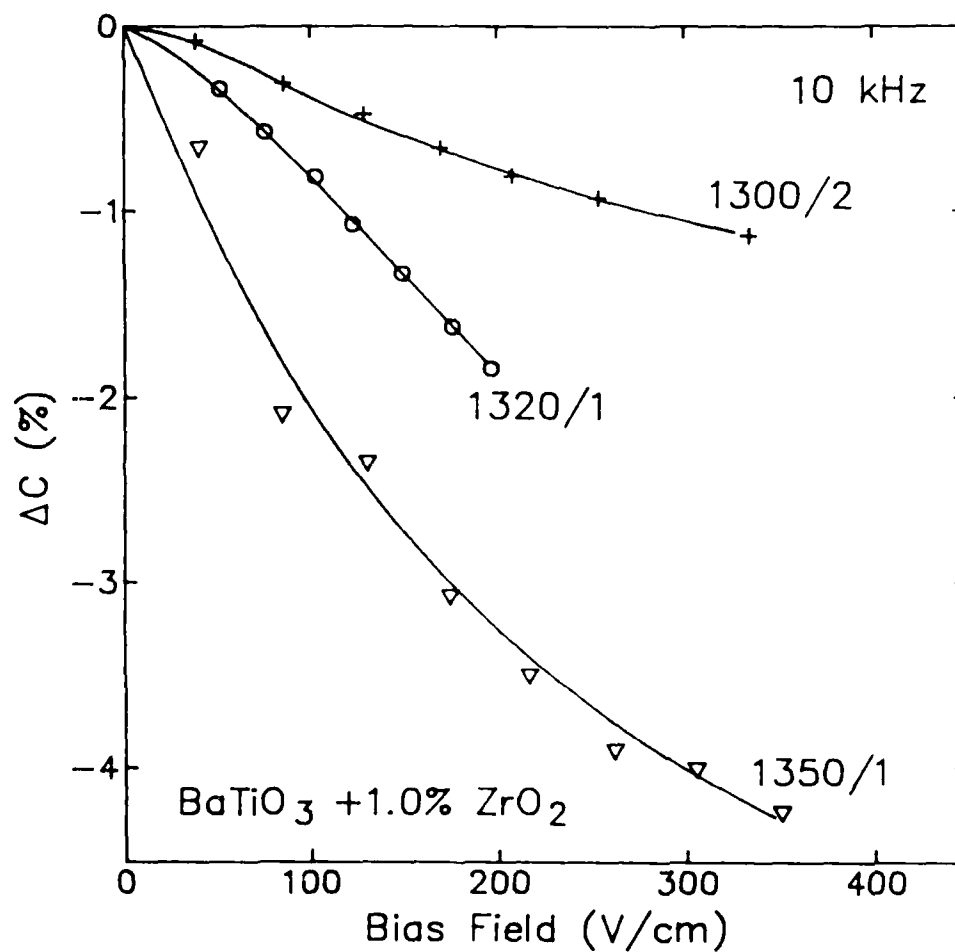


Figure 11. Change in capacitance as a function of bias field for BaTiO<sub>3</sub> with 1.0 wt% added zirconia.

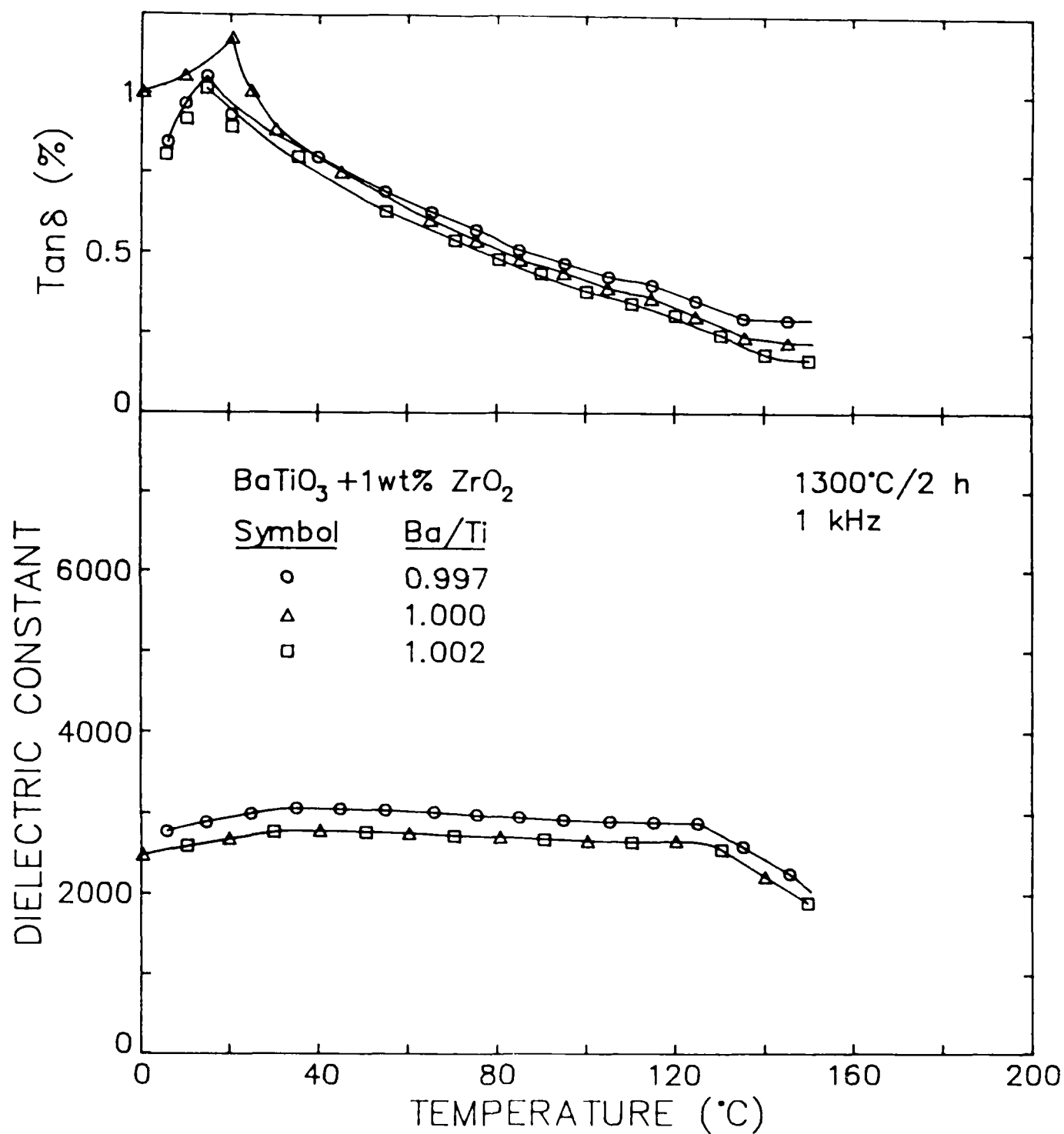


Figure 12. Dielectric response of  $\text{BaTiO}_3$  (1.0 wt% added  $\text{ZrO}_2$ ) with varying Ba/Ti atomic ratios 0.997, 1.000 and 1.002 sintered at 1300°C/2h.

## Technical Reports

1. R. C. Buchanan, "Property/Composition Relationships in Multicomponent Glasses", University of Illinois, Urbana, August 1975.
2. R. C. Buchanan, "Computerized Study of Glass Properties in Complex Lead Borosilicate Glasses", University of Illinois, Urbana, April, 1975.
3. R. C. Buchanan, "Crystallization in Lead Borosilicate Glasses", University of Illinois, Urbana, August, 1977.
4. R. C. Buchanan and J. Bukowski, "Lead Borosilicate Glasses for Low Temperature Dielectric Insulation on Al Substrates", University of Illinois, Urbana, March 1979.
5. D. E. Wittmer and R. C. Buchanan, "Densification of PZT Ceramics with  $V_2O_5$  Additive", (ONR Report #1), University of Illinois, Urbana, January 1979.
6. H. D. Deford and R. C. Buchanan, "Low Temperature Densification of  $ZrO_2$  with Vanadate Additive", (ONR Report #2), University of Illinois, Urbana, July 1979.
7. A. Sircar and R. C. Buchanan, "Densification of Zirconia with Borates", (ONR Report #3), University of Illinois, Urbana, January 1980.
8. R. C. Buchanan and H. D. Deford, "Densification of Monoclinic  $ZrO_2$  with Vanadate Additives", (ONR Report #4), University of Illinois, Urbana, July 1982.
9. R. C. Buchanan and S. Pope, "Optical and Electrical Properties of Yttria Stabilized Zirconia (YSZ) Crystals," (ONR Report #5), University of Illinois, Urbana, September 1981.
10. R. C. Buchanan and J. Boy, "Effect of Coprecipitation Parameters on Powder Characteristics and on Densification of PZT Ceramics", (ONR Report #6), University of Illinois, Urbana, September 1982.
11. R. C. Buchanan and D. M. Wilson, "Densification of Precipitated Yttria Stabilized Zirconia (YSZ) to Achieve Translucent Properties", (ONR Report #7), University of Illinois, Urbana, November 1982.
12. R. C. Buchanan and D. M. Wilson, "Role of  $Al_2O_3$  in Sintering of Submicron Yttria Stabilized  $ZrO_2$  Powders", (ONR Report #8), University of Illinois, Urbana, December 1983.

13. R. C. Buchanan and D. M. Wilson, "Densification of Submicron YSZ Powders with Alumina and Borate Additives", (ONR Report #9), University of Illinois, Urbana, December 1984.
14. R. C. Buchanan and J. Boy "Effect of Powder Characteristics on Microstructure and Properties in Alkoxide Prepared PZT Ceramics", (ONR Report #10), University of Illinois, Urbana, July 1984.
15. R. C. Buchanan and W. W. Davison, "Influence of Alumina on the Structure and Mechanical Properties of Yttria Stabilized Zirconia Composites", (ONR Report #11), University of Illinois, Urbana, July 1985.
16. R. C. Buchanan and A. K. Maurice, "Preparation and Stoichiometry Effects on Microstructure and Properties of High Purity BaTiO<sub>3</sub>", (ONR Report #12), University of Illinois, Urbana, March 1986.
17. R. C. Buchanan and W. W. Davison, "Influence of Al<sub>2</sub>O<sub>3</sub> on Properties of Yttria Stabilized Zirconia-Al<sub>2</sub>O<sub>3</sub> Composites," (ONR Report #13), University of Illinois, Urbana, March 1986.
18. R. C. Buchanan and T. R. Armstrong, "Processing and Additive Effects of ZrO<sub>2</sub> on Microstructure and Dielectric Properties of BaTiO<sub>3</sub> Ceramics", (ONR Report #14), University of Illinois, Urbana, December 1987.

END

DATE

FILMED

DTIC

JULY 88